Three-dimensional hybrid nanofluid along a stretching/ shrinking sheet: Application of Al_2O_3-Cu

S. Ahmed[1], K. Badak[2] and R.P. Sharma[3]

[1]*Department of Mathematics, Rajiv Gandhi University, Rono Hills, Doimukh, Arunachal Pradesh, India, Pin-791112*
[2]*Department of Basic and Applied Science, NIT Arunachal Pradesh, Jote, Papum Pare District, Arunachal Pradesh-791113*
[3]*Department of Mechanical Engineering, NIT Arunachal Pradesh, Jote, Papum Pare District, Arunachal Pradesh-791113*
***Corresponding author**: nanofluid.sahin@gmail.com; badakkirnu@gmail.com; rpsharma@nitap.ac.in

ABSTRACT The three-dimensional flow of a hybrid nanofluid over a stretching/shrinking sheet including copper and alumina nanoparticles in ethylene glycol has been investigated under the influence of magnetic field, thermal radiation, joule heating, convective conditions, and slip boundary conditions. Hybrid nanofluids disperse two distinct nanoparticles in a fluid, providing better heat conductivity for industrial applications. Using the bvp4c technique, non-linear partial differential equations are transformed into non-linear ordinary differential equations with similarity variables. Velocity profile declines with higher magnetic, suction, and slip parameter values, while sheet temperature profile growths with Biot, Eckert, and radiative parameters. The study discovers that a stronger magnetic force enhances temperature across a stretched sheet but has the reverse impact on a shrinking sheet. The novelty lies in using a three-dimensional model for this investigation, providing more accurate and realistic representations of fluid flow and heat transport compared to conventional two-dimensional models. In contrast to the earlier experiment, ethylene glycol, the base fluid, and three-dimensional flow are both taken into account, along with alumina and copper nanoparticles scattered in it. Quantitative analysis of the results demonstrates that in hybrid nanofluids, a higher Biot number and Reynolds number result in a faster rate of heat transfer.

KEYWORDS Hybrid nanofluid; Stretching/Shrinking sheet; Slip condition; Convective condition; MHD

1. Introduction

The role of the heating or cooling agent is of the utmost significance in many thermal engineering applications. Conventional fluids like water, engine oil, ethylene glycol, etc. provide a limited source of heating and cooling in end products. (Choi and Eastman, 1995) introduced the term "nanofluid", which offers a higher rate of heat transfer as compared to conventional fluids. The dispersion of nanosized (1–100 nm) particles in a conventional fluid is termed nanofluid. Further, the thermal conductivity of nanofluids is extended by adding two or more nanoparticles to conventional fluids, which are then called hybrid nanofluids. These fluids provide superior thermal efficiency characteristics compared to nanofluids and conceal the synergistic effects that are used in a variety of heat transfer phenomena, including biomedicine, electronic cooling, refrigeration, transformer cooling, etc. Rashad et al. (2018); Mahdy et al. (2021); Alarabi et al. (2021); El-Zahar et al. (2021); Sheikholeslami (2022c,a,b, 2023), and Sheikholeslami and Al-Hussein (2023), as well as Pattnaik et al. (2020, 2021, 2022) and Jena et al. (2020), have all investigated the applications and significance of various forms of hybrid nanofluid.

Heat transportation in the physical models depends mostly on the surface of the problems. The stretching or shrinking surface plays a vital role in various fields like hot rolling, cooling a metallic plate in a cooling shower, etc. The concept of fluid flow over a moving solid material was first studied by Sakiadis (1961). Crane (1970) examined the two-dimensional flow over a stretching surface. The impact of heat source/sink and thermal radiation was studied by Sharma et al. (2019) over a porous shrinking surface due to the motion of the nanofluid flow. Mishra et al. (2019) studied the behaviour of power-law fluid with a non-uniform heat source and MHD over a stretching sheet. In addition, taking into account the convective sheet's stretching and contracting shows that the fluid's temperature and thermal efficiency have improved. Waqas et al. (2022) use computer simulations to compare the influence of the convective surface with a magnetic field, joule heating, thermal radiation, viscous dissipation, and heat source/sink for various nanoparticles (alumina, copper, and graphene oxide). Sagheer et al. (2023) investigated the two-dimensional Maxwell hybrid nanofluid flow under the influence of a magnetic field, viscous dissipation, and a heat source or sink in porous media. They focused on a convective, linearly extending surface. They discovered that the increased value of the Biot number tends to increase the temperature gradient using the bvp4c algorithm in the MATLAB software.

No-slip boundary conditions are obviously not applicable to all models. As a result of the numerous uses of slip boundary conditions in the cleaning of mechanical heart valves, micro pumps, micro-nozzles, hard disc

DOI: 10.52292/j.laar.2024.3135
Received: February 21, 2023.
Accepted: August 8, 2023.
Recommended by Germán Prieto.

drives, the perfection of cavities, etc., many researchers have focused on these effects. Bhattacharyya et al. (2011) considered the effects of slip conditions near the stagnation point on the boundary layer of the shrinking sheet in their investigation. The consequences of slip effects due to three-dimensional flow towards a permeable stretching or shrinking sheet have been examined by Jusoh et al. (2018). Mahabaleshwar et al. (2020) worked on the Newtonian flow field on Permeable stretching and shrinking surfaces by considering slip conditions. The effects of slip and convective conditions have been analysed by Khashi'ie et al. (2020b) in a three-dimensional flow of copper-alumina and water over a permeable stretching or shrinking surface. They conclude that with the increment of the Biot number and slip parameter, there is a higher rate of heat transfer. When silver oxide and iron oxide are suspended over a convective stretchable surface, Rashmi et al. (2022) examine the impact of slip boundary conditions and a magnetic field. Their findings show that the slip parameter decreases fluid flow. Areekara et al. (2023) and numerous other studies studied the impact of slip situations on various surfaces by taking different nanoparticles into consideration.

Magnetohydrodynamics (MHD) is the study of fluid dynamics in the presence of a magnetic field. Many researchers recognised that the hybrid nanofluids offered better heat transfer along with MHD in fluid flow. Thus, the effects of MHD are applicable in the polymer industry, solar collectors, chemical engineering, etc. Devi and Devi (2016a,b) numerically investigated the effects of MHD, Newtonian heating in the three-dimensional flow of hybrid nanofluid over a stretching or shrinking surface, and suction in the two-dimensional flow over a permeable stretching or shrinking sheet of copper-alumina/water. Jamaludin et al. (2018) worked on three-dimensional flow by considering permeable stretching and shrinking surfaces along with mixed convection, MHD, slip velocity, and thermal slip. In the studies cited by Ebaid et al. (2014); Jusoh et al. (2017); Aly and Pop (2019); Khashi'ie et al. (2020a); Jamaludin et al. (2020); El-Zahar et al. (2020); Kumbhakar and Nandi (2022); Jaafar et al. (2022) and El-Zahar et al. (2022) the behaviour of the MHD fluid molecules is investigated.

Copper nanoparticles act as anti-microbials, antibiotics, etc., and they are used in many fields like microelectronic devices and optical due to their low cost, high thermal conductivity, and electrical potential. On the other hand, alumina nanoparticles improve melting points and high-temperature resistance. In light of the aforementioned literature review and the applications of nanoparticles, it is discovered that the effects of a magnetic field, thermal radiation, joule heating, convective heating, and slip boundary conditions due to a three-dimensional flow field through a stretching or shrinking sheet with suspended alumina and copper nanoparticles in ethylene glycol as a base fluid have not yet been investigated. In order to close this research gap, the current numerical computation was made.

The originality of this investigation is to introduce the influence of a magnetic field on the hybrid nanofluid flow under the action of shrinking and stretching. However, adding a magnetic field perpendicular to the stretching or shrinking sheet can induce magneto-hydrodynamic (MHD) effects, altering the flow patterns and heat transfer rates significantly, and this is particularly relevant to applications in magnetic cooling or magnetic fluid-based devices. Using a similarity variable, the basic governing equations of the proposed model are reframed into a system of dimension-one on-line ordinary differential equations and then numerically computed using the bvp4c algorithm in the MATLAB software. With the following research inquiries, physical parameters are discussed:

1. The three-dimensional modelling of such flows, which can provide more precise predictions of flow behaviour and heat transfer characteristics, has a research deficit.
2. A unique contribution to the literature would be to comprehend how the stretching and shrinking processes interact, affect the flow field, and affect heat transmission.
3. What effects do the magnetic parameter, Biot number, and slip parameter have on the hybrid nanofluid's velocity and temperature?
4. What role does the Biot number play in the transfer of heat?
5. How does the volume fraction of nanoparticles affect the temperature and velocity profiles?
6. How do sheets that are stretching and contracting react in the flow field?

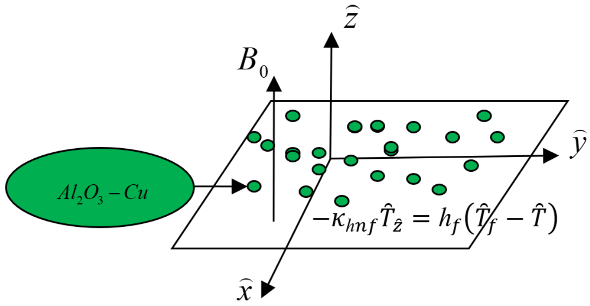

Figure 1: Geometry of the flow model.

2. Problem formulation

In Figure 1, consider a steady, incompressible three-dimensional flow field over a stretching or shrinking sheet with copper and alumina nanoparticles suspended in ethylene glycol as the base fluid, $\hat{u}_w(\hat{x}) = a\hat{x}$ and $\hat{v}_w(\hat{x}) = a\hat{y}$, where a is a positive constant, and $\hat{u}_w(\hat{x})$ and $\hat{v}_w(\hat{x})$ are the velocities at the wall along $\hat{x}$ and $\hat{y}$ direction, respectively. The domain of the flow field occupies the regions, $\hat{z} \geq 0$ and $\hat{x}\hat{y}-$planes as stretching or shrinking surfaces with slip boundary conditions, thermal radiation, and joule heating. Further, the convective condition is considered at the bottom of the sheet, which provides heat transfer coefficients h_f, due to constant temperature $\hat{T}_f$, and the influences of agglomeration due to hybridization are neglected. In addition, a homogeneous magnetic field of

high magnetic flux density B_0 is applied perpendicular to the plane. According to Khashi'ie et al. (2020b); Devi and Devi (2016a), and Kumar et al. (2018), the fundamental non-linear partial differential equation governing mass, momentum, and energy conservation is as follows:
Continuity equation:

$$\frac{\partial \hat{u}}{\partial \hat{x}}+\frac{\partial \hat{v}}{\partial \hat{y}}+\frac{\partial \hat{w}}{\partial \hat{z}}=0 \tag{1}$$

Momentum equation:

$$\hat{u}\frac{\partial \hat{u}}{\partial \hat{x}}+\hat{v}\frac{\partial \hat{u}}{\partial \hat{y}}+\hat{w}\frac{\partial \hat{u}}{\partial \hat{z}}=\frac{\mu_{hnf}}{\rho_{hnf}}\frac{\partial^2 \hat{u}}{\partial \hat{z}^2}-\frac{\sigma_{hnf}}{\rho_{hnf}}B_0^2\hat{u} \tag{2}$$

$$\hat{u}\frac{\partial \hat{v}}{\partial \hat{x}}+\hat{v}\frac{\partial \hat{v}}{\partial \hat{y}}+\hat{w}\frac{\partial \hat{v}}{\partial \hat{z}}=\frac{\mu_{hnf}}{\rho_{hnf}}\frac{\partial^2 \hat{v}}{\partial \hat{z}^2}-\frac{\sigma_{hnf}}{\rho_{hnf}}B_0^2\hat{v} \tag{3}$$

Energy equation:

$$\begin{aligned}\hat{u}\frac{\partial \hat{T}}{\partial \hat{x}}+\hat{v}\frac{\partial \hat{T}}{\partial \hat{y}}+\hat{w}\frac{\partial \hat{T}}{\partial \hat{z}}&=\frac{\kappa_{hnf}}{(\rho C_p)_{hnf}}\frac{\partial^2 \hat{T}}{\partial \hat{z}^2}\\&-\frac{1}{(\rho C_p)_{hnf}}\frac{\partial}{\partial \hat{z}}\left(-\frac{16\sigma^*\hat{T}_\infty^3}{3\kappa^*}\right)\frac{\partial \hat{T}}{\partial \hat{z}}\\&+\frac{\sigma_{hnf}}{(\rho C_p)_{hnf}}B_0^2\left(\hat{u}^2+\hat{v}^2\right)\end{aligned} \tag{4}$$

With boundary conditions (Khashi'ie et al., 2020b)

$$\left.\begin{aligned}&\hat{u}=\hat{u}_w(\hat{x})\lambda+B_0\frac{\partial \hat{u}}{\partial \hat{z}},\ \hat{v}=\hat{v}_w(\hat{y})\lambda+B_0\frac{\partial \hat{v}}{\partial \hat{z}},\\&\hat{w}=\hat{w}_0,\ -\kappa_{hnf}\frac{\partial \hat{T}}{\partial \hat{z}}=h_f\left(\hat{T}_f-\hat{T}\right)\ \text{at } \hat{z}=0\\&\hat{u}\to 0,\ \hat{v}\to 0,\ \hat{T}\to \hat{T}_\infty \text{ as } \hat{z}\to\infty\end{aligned}\right\} \tag{5}$$

Here, $\lambda>0$ for stretching sheet, $\lambda=0$ for static sheet and $\lambda<0$ denotes shrinking sheet, respectively. $\hat{w}_0>0$ for injection and $\hat{w}_0<0$ defines suction, respectively. $q_r=-\frac{16\sigma^*\hat{T}_\infty^3}{3\kappa^*}\frac{\partial \hat{T}}{\partial \hat{z}}$ is the term denoted for radiative heat flux by the linear Rosseland approximation, such as κ^* and σ^* defines mean absorption coefficients and the Stefan-Boltzmann constant, respectively. In the proposed model, temperature differences are assumed to be very small within the fluid flow. Thus, using Taylor's expansion, T^4 may be written as $T^4\equiv 4T_\infty^3T-3T_\infty^4$ (neglecting higher-order terms).

Introducing dimensionless similarity variables (Khashi'ie et al., 2020b) to obtain ordinary differential equations as follows:

$$\left.\begin{aligned}&\eta=\hat{z}\sqrt{a/\nu_f},\ \hat{u}=a\hat{x}f'(\eta),\ \hat{v}=a\hat{y}h'(\eta),\\&\hat{w}=-\sqrt{a\nu_f}[f(\eta)+h(\eta)],\ \theta(\eta)=\frac{\hat{T}-\hat{T}_\infty}{\hat{T}_f-\hat{T}_\infty}\end{aligned}\right\} \tag{6}$$

So that,

$$\hat{w}_0=-\sqrt{a\nu_f}S \tag{7}$$

Obtained non-linear ordinary differential equations by applying Eq. 6 in Eqs. 1-5 are as follows:

$$\frac{\gamma_1}{\gamma_2}f'''+(f+h)f''-f'^2-\frac{\gamma_3}{\gamma_2}Mf'=0 \tag{8}$$

$$\frac{\gamma_1}{\gamma_2}h'''+(f+h)h''-h'^2-\frac{\gamma_3}{\gamma_2}Mh'=0 \tag{9}$$

$$\begin{aligned}&\left(\gamma_4+\frac{4}{3}R\right)\theta''+Pr\gamma_5(f+h)\theta'+\\&\qquad\gamma_3PrM\left(Ec_xf'^2+Ec_yh'^2\right)=0\end{aligned} \tag{10}$$

With boundary conditions

$$\left.\begin{aligned}&f(0)=S,\ f'(0)=\lambda+\beta f'(0),\ h(0)=0,\\&h'(0)=\lambda+\beta h'(0),\ -\gamma_4\theta'(0)=Bi[1-\theta(0)]\\&f'(\eta)\to 0,\ h'(\eta)\to 0,\ \theta(0)\to 0 \text{ as } \eta\to\infty\end{aligned}\right\} \tag{11}$$

Here,

$$\begin{aligned}&\gamma_1=\frac{\mu_{hnf}}{\mu_f},\ \gamma_2=\frac{\rho_{hnf}}{\rho_f},\ \gamma_3=\frac{\sigma_{hnf}}{\sigma_f},\ \gamma_4=\frac{\kappa_{hnf}}{\kappa_f},\\&Bi=\frac{h_f}{\kappa_f}\sqrt{\frac{\nu_f}{a}},\ \gamma_5=\frac{(\rho C_p)_{hnf}}{(\rho C_p)_f},\ Pr=\frac{(\mu C_p)_f}{\kappa_f},\\&M=\frac{\sigma_fB_0^2}{\rho_fa},\ R=\frac{4\sigma^*\hat{T}_\infty^3}{\kappa^*\kappa_f},\ Ec_x=\frac{\hat{u}_w^2}{(C_p)_f\left(\hat{T}_f-\hat{T}_\infty\right)},\\&\beta=\beta_0\sqrt{\frac{a}{\nu_f}},\ Ec_y=\frac{\hat{v}_w^2}{(C_p)_f\left(\hat{T}_f-\hat{T}_\infty\right)}\end{aligned}$$

and Pr, M, R, Ec_x, Ec_y, Bi and β are the non-dimensional parameters as Prandtl number, Magnetic parameter, radiative parameter, Eckert number along $\hat{x}$ and $\hat{y}$ direction, Biot number and velocity slip parameter, respectively.

The relationship between the thermophysical properties of nanofluid and hybrid nanofluid (Rostami et al., 2018) is defined as

$$\begin{aligned}&\mu_{hnf}=\frac{\mu_f}{(1-\phi_1)^{2.5}(1-\phi_2)^{2.5}},\\&\rho_{hnf}=\phi_2\rho_{Cu}+(1+\phi_2)\left[(1-\phi_1)\rho_f+\phi_1\rho_{Al_2O_3}\right],\\&\kappa_{nf}=\frac{\kappa_{Al_2O_3}+2\kappa_f-2\phi_1\left(\kappa_f-\kappa_{Al_2O_3}\right)}{\kappa_{Al_2O_3}+2\kappa_f+2\phi_1\left(\kappa_f-\kappa_{Al_2O_3}\right)}\times\kappa_f,\\&\kappa_{hnf}=\frac{\kappa_{Cu}+2\kappa_{nf}-2\phi_2\left(\kappa_{nf}-\kappa_{Cu}\right)}{\kappa_{Cu}+2\kappa_{nf}+2\phi_2\left(\kappa_{nf}-\kappa_{Cu}\right)}\times\kappa_{nf},\\&\sigma_{nf}=\frac{2\sigma_f+\sigma_{Al_2O_3}-2\phi_1\left(\sigma_f-\sigma Al_2O_3\right)}{2\sigma_f+\sigma Al_2O_3+\phi_1\left(\sigma_f-\kappa_{Al_2O_3}\right)}\times\sigma_f,\\&\sigma_{hnf}=\frac{2\sigma_{nf}+\sigma_{Cu}-2\phi_2\left(\sigma_{nf}-\sigma_{Cu}\right)}{2\sigma_{nf}+\sigma_{Cu}+2\phi_2\left(\sigma_{nf}-\sigma_{Cu}\right)}\times\sigma_{nf},\\&(\rho C_p)_{hnf}=\phi_2(\rho C_p)_{Cu}\\&\qquad+(1-\phi_2)\left[(1-\phi_1)(\rho C_p)_f+\phi_1(\rho C_p)_{Al_2O_3}\right]\end{aligned}$$

Shear stress $\tau_{w\hat{x}}=\frac{\partial \hat{u}}{\partial \hat{z}}|_{\hat{z}=0}$ along de $\hat{x}$-direction and $\tau_{w\hat{y}}=\frac{\partial \hat{v}}{\partial \hat{z}}|_{\hat{z}=0}$ along de $\hat{y}$-direction, respectively while $q_w=-\kappa_{hnf}\frac{\partial \hat{T}}{\partial \hat{z}}|_{\hat{z}=0}+q_r|_{\hat{z}=0}$ is the heat flux on the stretching/shrinking surface. Thus, the respective skin friction

Table 1: Values of thermophysical properties for $C_2H_6O_2$, Al_2O_3 and Cu (Khashi'ie et al., 2020a; Hosseinzadeh et al., 2018; Hafeez et al., 2021).

Traits	$C_2H_6O_2$	Al_2O_3	Cu
ρ (kg/m^3)	1115	3970	8933
κ (W/mK)	0.253	40	400
σ (s/m)	1.10×10^{-4}	35×10^{-6}	5.96×10^{-6}
C_p (J/kgK)	3430	765	385

Table 2: Comparative values for $-f''(0)$ and $-h''(0)$, $S=\beta=Bi=\phi_1=\phi_2=M=R=Ec_x=Ec_y=0$, $\lambda=1$.

	HAM solution	bvp4c solution	Present solution
$-f''(0)$	1.73722	1.73722	1.73722
$-h''(0)$	1.73722	1.73722	1.73722

Table 3: Grid point stability test.

	$h=0.001$		$h=0.01$	
η	$f'(\eta)$	$\theta(\eta)$	$f'(\eta)$	$\theta(\eta)$
0	0.7601	0.0491	0.7608	0.0491
0.4990	0.4386	0.0134	0.4399	0.0138
0.8990	0.1792	0.0065	0.1798	0.0069
1.4990	0.0480	0.0017	0.0491	0.0018
1.7990	0.0169	0.0002	0.0170	0.0001
1.9880	0.0010	0.0000	0.0010	0.0000
2.0000	0.0000	0.0000	0.0000	0.0000

coefficient and local Nusselt number (Khashi'ie et al., 2020b; Kumar et al., 2018) are defined as follows:

$$C_{f\hat{x}}=\frac{\tau_{w\hat{x}}}{\rho_f\hat{u}_w^2},\ C_{f\hat{y}}=\frac{\tau_{w\hat{y}}}{\rho_f\hat{v}_w^2},\ Nu_{\hat{x}}=-\frac{\hat{x}q_w}{\kappa_f\left(\hat{T}_f-\hat{T}_\infty\right)} \tag{12}$$

by applying (7) in (12), we get

$$(Re_{\hat{x}})^{0.5}C_{f\hat{x}}=\frac{\mu_{hnf}}{\mu_f}f''(0),\ (Re_{\hat{y}})^{0.5}C_{f\hat{y}}=\frac{\mu_{hnf}}{\mu_f}h''(0),$$
$$(Re_{\hat{x}})^{-0.5}Nu_{\hat{x}}=-\left(\frac{\kappa_{hnf}}{\kappa_f}+\frac{4}{3}R\right)\theta'(0) \tag{13}$$

where $Re_{\hat{x}}=\frac{\hat{u}_w\hat{x}}{\nu_f}$ and $Re_{\hat{y}}=\frac{\hat{v}_w\hat{y}}{\nu_f}$ signifies the local Reynolds number and f', h' defines it as a derivative of f and h with respect to η.

3. Validation and accuracy of the proposed problem

Using the bvp4c algorithm in the MATLAB software, a finite difference approach has been utilized to determine the numerical solutions of dimensionless non-linear ordinary differential equations derived via suitable dimensionless similarity variables with boundary conditions. This numerical technique uses a three-stage Labatto IIIa finite difference algorithm. This approach was developed by Shampine et al. (2003) to assess nonlinear ordinary differential equations. The results of the current numerical computation using the thermophysical characteristics listed in Table 1 showed good agreement with earlier research using the Homotopy Analysis Method (HAM) and bvp4c in Hayat et al. (2015) and Khashi'ie et al. (2020b), respectively. This is shown in Table 2. These correlations demonstrate the validity of the current issue with respect to the thermophysical characteristics listed in Table 1 and give the bvp4c algorithm accuracy.

The grid-point stability test of the current inquiry is shown in Table 3. According to Table 3, any physical variable's variation between $h=0.001$ and $h=0.01$ step sizes is less than 10^{-3}, sustaining asymptotic flow behaviour due to boundary conditions. As a result, the finite difference numerical approach implemented using the built-in Matlab bvp4c is stable and convergent.

4. Results and discussion

Physical parameters of the non-dimensional ordinary differential equations 8-10 with boundary conditions 11 are computed by finite difference via the bvp4c algorithm in MATLAB software. In this study, we fixed the Prandtl number $Pr=184.5$ and considered other variables parameters as $\phi_1=\phi_2=0.01$, $\beta=0.1$, $S=2$, $M=0.1$, $Bi=0.1$, $R=0.2$, $Ec_x=Ec_x=0.01$ and $\lambda=1$ for the stretching case and $\lambda=-1$ for the shrinking case, respectively. The behaviour of dimensionless velocity and temperature views for the distinct physical parameters is illustrated with graphs and tables.

Figure 2 displays the behaviour of distinct values of volume fraction of nanoparticles (copper and alumina) in a dimensionless velocity profile $f'(\eta)$ for the stretching case ($\lambda=1$). Physically, increasing the volume fraction of nanoparticles in a conventional fluid causes the hybrid nanofluid to become viscous, which reduces $f'(\eta)$. Figure 3 displays the behaviour of alumina and copper nanoparticles during stretching and shrinking ($\lambda=-1$) of the sheet simultaneously. It is observed that for a higher volume fraction (ϕ), the velocity profile slows down as compared to the lowest volume fraction. Since nanoparticles Al_2O_3 (ϕ_1 =0.02, 0.03, 0.05) depict a lower velocity

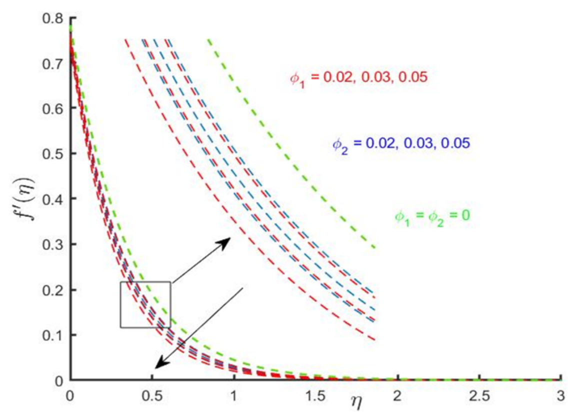

Figure 2: Behaviour of $f'(\eta)$ for distinct volume fractions of alumina and copper.

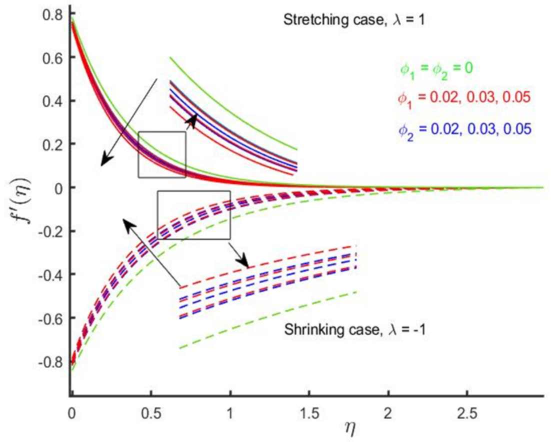

Figure 3: Behaviour of $f'(\eta)$ for distinct volume fraction of alumina and copper.

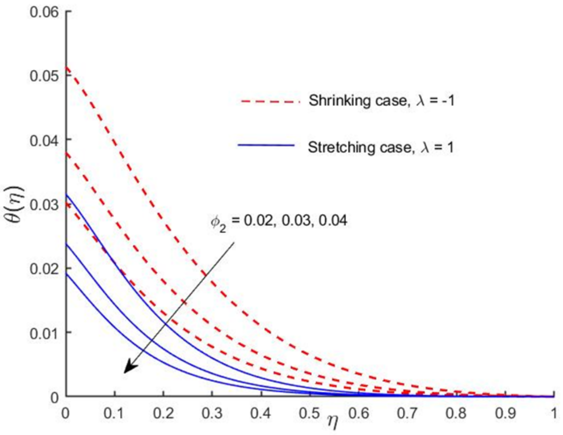

Figure 4: Behaviour of $\theta(\eta)$ for distinct volume fraction of copper.

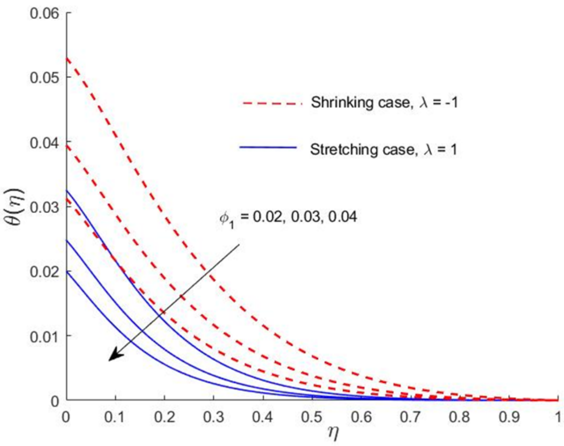

Figure 5: Behaviour of $\theta(\eta)$ for distinct volume fraction of alumina.

side view than Cu (ϕ_2 =0.02, 0.03, 0.05) nanoparticles in the stretching ($\lambda = 1$), when alumina particles are added instead of copper nanoparticles, viscosity increases. On the other hand, it shows the opposite behaviour for the shrinking ($\lambda = -1$) case. Figure 4 and Fig. 5 illustrate the behaviour of volume fractions of copper (ϕ_2 =0.02, 0.03, 0.04) and alumina (ϕ_1 =0.02, 0.03, 0.04) nanoparticles in base fluid due to stretching and shrinking. From the plotted graphs, it is observed that dimensionless temperature $\theta(\eta)$ profiles decrease with the higher amount of nanoparticles in the fluid molecules. Physically, the viscosity of the fluid and its temperature have an inverse connection; hence, a higher volume percentage tends to slow the fluid's temperature distribution.

As a result, a lot of industrial equipment uses nanoparticles as a cooling agent. The temperature of the fluid molecule has a better influence in the shrinking ($\lambda = -1$) case than the stretching ($\lambda = 1$) case while increasing the volume fraction of copper and alumina in the base fluid. Therefore, fluid molecules provide better thermal energies in the shrinking case as compared to the stretching case.

The magnetic parameter (M) is one of the dimensionless parameters in the proposed model, which describes the impact of a uniform magnetic field of strength (B_0) in fluid flow. Figure 6 depicts the impact of the magnetic parameter (M =0, 1, 2, 3) on the main dimensionless velocity profile $f'(\eta)$ for the stretching/shrinking case. It is observed that the primary velocity of the fluid molecules reduces with increasing values of M. In the stretching sheet, the lowest value of offers lower resistivity to electrically conducting hybrid nanofluid due to Lorentz's force, while

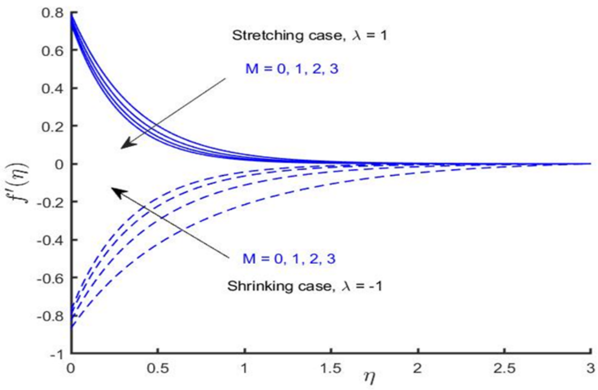

Figure 6: Behaviour of $f'(\eta)$ for distinct magnetic parameter.

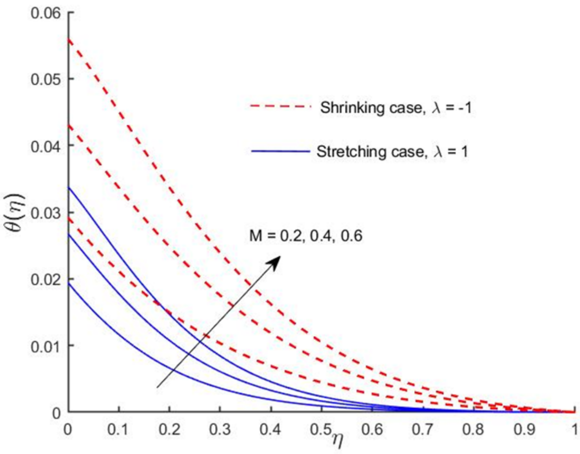

Figure 7: Behaviour of $\theta(\eta)$ for distinct magnetic parameter.

higher values of the magnetic parameter offer higher resistivity to electrically conducting hybrid nanofluid. Thus, it makes a thinner momentum boundary layer with the increment of a magnetic parameter in the case of stretching ($\lambda = 1$), while it shows the opposite behaviour in the shrinking ($\lambda = -1$) case. Lorentz's force, often known as the drag force, is a physical force that tends to oppose the flow. This force is used to control the flow field, which is particularly beneficial in the metal and electromagnetic coating of wires, among other applications. Figure 7 depicts the behaviour of magnetic parameters in a dimensionless temperature $\theta(\eta)$ profile due to the presence of copper ($\phi_2 = 0.01$) and alumina ($\phi_1 = 0.01$) nanoparticles in ethylene glycol as a base fluid over a stretching or shrinking sheet. The impact of M =0.2, 0.4, 0.6 on $\theta(\eta)$ over a shrinking sheet provides better thermal energies for fluid molecules as compared to stretching surfaces. It is observed that the thickness of the thermal boundary layer increases with the increment of magnetic parameters over a stretching sheet while showing the opposite behaviour in a shrinking sheet. Actually, the interaction between a conducting fluid and a nanoparticle produces a drag force when a magnetic field is applied. Fluid molecules produce heat in response to that force, which causes the temperature profile to climb. The properties of heat transmission on the stretched sheet are directly impacted by the hybrid-nanofluid's temperature. Heat transfer from the sheet to the fluid can be improved by regulating the fluid's temperature. In applications like cooling or heating operations, where effective heat transfer is crucial for achieving optimum performance, this is very useful. Figure 8 depicts the behaviour of slip parameters (β =0, 0.1, 0.3, 0,5) in dimensionless primary velocity profiles over a stretching or shrinking surface in the presence of alumina ($\phi_1 = 0.01$) and copper ($\phi_2 = 0.01$) nanoparticles and water as a base fluid. A lower value of β =0, 0.1 offers the least action of resistive force to the fluid molecules and then gradually increases its resistivity for $\beta = 0.5$. Naturally, the slip parameter offers resistive force to the fluid molecules and is hence $f'(\eta)$ reduced for a higher value of β over a stretching ($\lambda = 1$) surface, while hybrid nanofluid offers the opposite behaviour over a shrinking ($\lambda = -1$) surface.

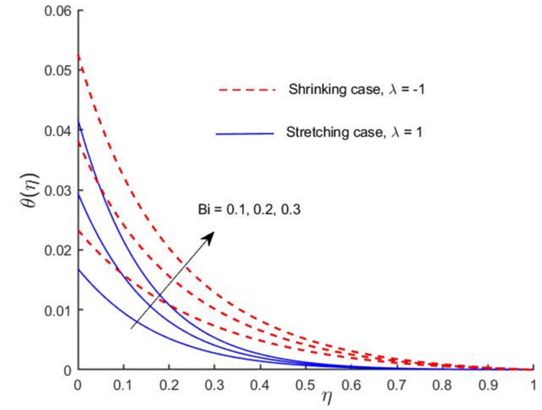

Figure 10: Behaviour of $\theta(\eta)$ for distinct Biot number.

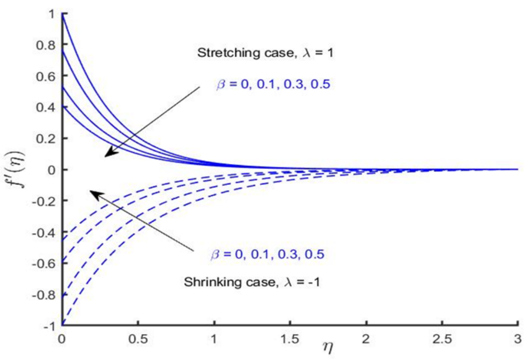

Figure 8: Behaviour of $f'(\eta)$ for distinct slip parameter.

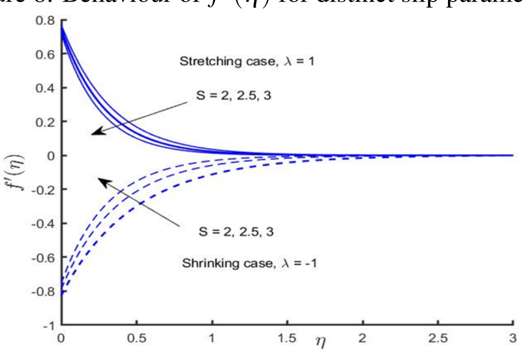

Figure 9: Behaviour of $f'(\eta)$ for distinct suction parameter.

The suction parameter is one of the dimensionless parameters that helps control the hybrid nanofluid flow. It aims to reduce the drag force due to external flow, reducing the velocity of the fluid molecules. Figure 9 depicts the behaviour of the primary velocity profile due to the influence of the suction parameter (S =2, 2.5, 3) over the stretching or shrinking surface. It is observed that the primary velocity profile decreases for a maximum amount of suction while offering a rise in $f'(\eta)$ over a stretching surface and a shrinking surface, respectively. Since the sheet is heated from the bottom, and then its influences due to the Biot number (Bi =0.1, 0.2, 0.3) are depicted in Fig. 10. The lowest value of the Biot number $Bi = 0.1$ offers lower thermal energies to the fluid molecules, while a higher value of $Bi = 0.3$ provides better thermal energies, which boost the thermal conductivity of the fluid molecules due to a raise in convective heat. Convective plates in fluid mechanics transmit heat to the fluid, raising its temperature as a result. It is observed that the influence of the Biot number results in better thermal conductivity over a shrinking surface as compared to a stretching surface.

The difference between the kinetic and enthalpy energies is known as the Eckert number (Ec_x, Ec_y). It denotes the loss of energy within fluid molecules. In Fig. 11, it can be seen that a larger magnitude of $Ec_x = Ec_y = 0.04$ causes the temperature profile to rise relative to a smaller value of $Ec_x = Ec_y = 0.02$. Furthermore, the temperature distribution caused by a contracting instance exhibits dominance over an expanding instance. The temperature profile climbs with the increment value of the Eckert num-

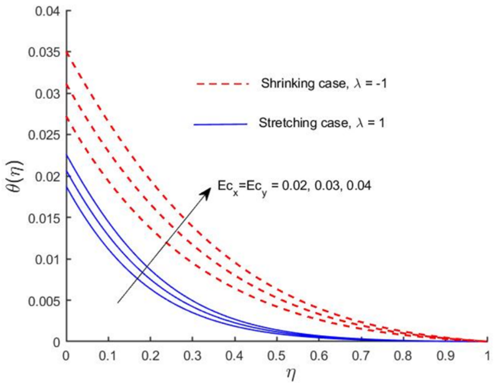

Figure 11: Behaviour of $\theta(\eta)$ for distinct Eckert number.

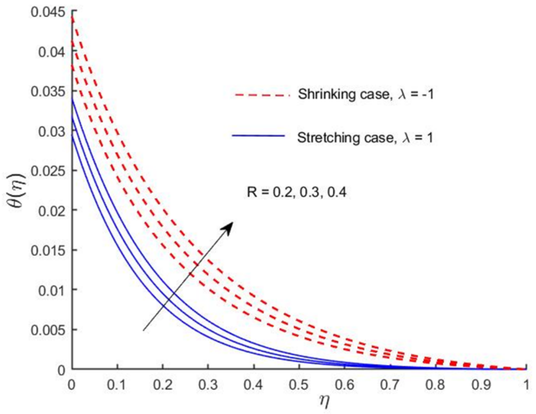

Figure 12: Behaviour of $\theta(\eta)$ for distinct radiative parameter.

ber because extra kinetic energy is physically stored as a result of frictional heating, which causes temperature profiles to climb. In Fig. 12, the impact of the thermal radiative parameter is shown. It is a phenomenon in nature when radiation enters a system and produces more kinetic energy, which raises the temperature profile of the fluid molecule. In biology, malignant cells can be killed by utilising the elevation of temperature caused by radiative effects in hybrid nanofluids.

Table 4 and Table 5 display the variations of skin friction coefficient for Reynolds numbers against magnetic parameters due to the stretching case and shrinking case, respectively. It is observed that the skin friction coefficient decreases with the increment values of magnetic drag force and Reynolds number over a stretching sheet, while the opposite behaviour occurs over a shrinking sheet. On the other hand, Tables 6 and 7 display the rate of heat transfer augmented with higher values of the Biot number and slip parameter against the Reynolds number over a stretching or shrinking sheet.

Table 4: Variation of Skin friction for stretching case.

	$Re=1$	$Re=5$	$Re=10$
$M=1$	-2.355	-1.0535	-0.7449
$M=5$	-2.8400	-1.2701	-0.8981
$M=10$	-3.2538	-1.4551	-1.0289

Table 5: Variation of Skin friction for shrinking case.

	$Re=1$	$Re=5$	$Re=10$
$M=1$	1.9425	0.8687	0.3124
$M=5$	2.6217	1.1725	0.8291
$M=10$	3.1195	1.3951	0.9865

Table 6: Variation of Nusselt number for stretching case.

	$Bi=0.3$	$Bi=1$	$\beta=0.3$	$\beta=1$
$Re=1$	0.3584	1.0972	0.1230	0.1233
$Re=10$	1.1332	3.4698	0.3889	0.3899

Table 7: Variation of Nusselt number for shrinking case.

	$Bi=0.3$	$Bi=1$	$\beta=0.3$	$\beta=1$
$Re=1$	0.3529	1.0645	0.1224	0.1231
$Re=10$	1.1161	3.3663	0.3869	0.3894

5. Conclusions

The employment of a three-dimensional model to analyse the behaviour of a hybrid nanofluid across a stretching or contracting sheet is an important novelty. Three-dimensional simulations can offer more accurate and realistic representations of fluid flow and heat transport phenomena than traditional two-dimensional models. The main findings of this investigation are summarized as follows:

- The viscosity of the hybrid nanofluid normally rises along with the volume fraction of nanoparticles. A higher viscosity than the base fluid alone is produced as a result of the increased flow resistance that nanoparticles add. A fluid with a higher viscosity typically has a slower flow rate.
- Hybrid-nanofluids are mixtures of a base fluid with nanoparticles as well as other additives. The fluid's thermal conductivity is greatly increased by the nanoparticles, which enhances the fluid's capacity for heat transmission. Applications like heat exchangers, cooling systems, and thermal management greatly benefit from this characteristic.
- The Biot number plays a significant role in determining the impact of convective heat transfer on the fluid temperature of a hybrid nanofluid.
- The boundary layer that forms close to the stretched sheet is affected by the fluid velocity in terms of thickness. The boundary layer becomes thinner with increased fluid velocity, lowering thermal resistance and boosting heat transmission. By doing this, the heat exchange between the sheet and the fluid can be accelerated and made more effective.
- $f'(\eta)$ profile reduces with the higher volume fractions of and nanoparticles in the base fluid ethylene glycol, for which the thickness of the momentum boundary is reduced.
- The temperature of the fluid molecules diminished by adding more nanoparticles (Cu-Al_2O_3) to the

fluid flow.
- M is a decreasing function of $f'(\eta)$ and an increasing function of $\theta(\eta)$, respectively.
- β and S are both declining functions of $f'(\eta)$.
- Convective situations cause the $\theta(\eta)$ profile to increase along with the Biot number.
- The Eckert number and radiative parameter grow, which causes $\theta(\eta)$ to rise.

Nomenclature

$\hat{u}$: Velocity component in $\hat{x}$– direction.
$\hat{v}$: Velocity component in $\hat{y}$– direction.
$\hat{w}$: Velocity component in $\hat{z}$– direction.
S: Constant mass flux parameter.
$\hat{T}$: Temperature.
Nu_x: Local Nusselt number.
C_{fx}: Skin coefficient friction along x direction.
C_{fy}: Skin coefficient friction along y direction.
C_p: Specific heat at constant temperature.
w_0: Mass flux.
Subscripts
w: Condition on wall.
∞: Ambient condition.
f: Base fluid.
nf: Nanofluid.
hnf: Hybrid nanofluid.
1: Alumina.
2: Copper.
Greek symbols
μ: Dynamic viscosity
ν: Kinematic viscosity
ρ: Density
θ: Dimensionless temperature
κ: Thermal conductivity
β_0: Slip length
η: Similarity variable
ϕ: Volume fraction
(ρC_P): Heat capacity

References

Alarabi, T. H., Rashad, A. M., and Mahdy, A. (2021). Homogeneous–heterogeneous chemical reactions of radiation hybrid nanofluid flow on a cylinder with joule heating: Nanoparticles shape impact. *Coatings*, 11(12):1490.

Aly, E. H. and Pop, I. (2019). MHD flow and heat transfer over a permeable stretching/shrinking sheet in a hybrid nanofluid with a convective boundary condition. *Int. J. Numer. Meth. Heat Fluid Flow*, 29(9):3012–3038.

Areekara, S., Sabu, A., Mathew, A., and Oke, A. (2023). Transport phenomena in Darcy-Forchheimer flow over a rotating disk with magnetic field and multiple slip effects: modified buongiorno nanofluid model. *Waves Random Complex Media*, pages 1–20.

Bhattacharyya, K., Mukhopadhyay, S., and Layek, G. (2011). Slip effects on boundary layer stagnation-point flow and heat transfer towards a shrinking sheet. *Int. J. Heat Mass Transf.*, 54(1-3):308–313.

Choi, S. U. S. and Eastman, J. A. (1995). Enhancing thermal conductivity of fluids with nanoparticles. In *ASME Int. Mech. Eng. Congr. Expo.*, San Francisco, CA, USA.

Crane, L. J. (1970). Flow past a stretching plate. *Z. Angew. Math. Physik ZAMP.*, 21(4):645–647.

Devi, S. P. A. and Devi, S. S. U. (2016a). Numerical investigation of hydromagnetic hybrid Cu – Al_2O_3/water nanofluid flow over a permeable stretching sheet with suction. *Int. J. Nonlinear Sci. Numer. Simul.*, 17(5):249–257.

Devi, S. S. U. and Devi, S. A. (2016b). Numerical investigation of hydromagnetic hybrid Cu – Al_2O_3/water nanofluid flow over a permeable stretching sheet with suction. *Can. J. Phys.*, 94(5):490–496.

Ebaid, A., Mutairi, F. A., and Khaled, S. M. (2014). Effect of velocity slip boundary condition on the flow and heat transfer of Cu-water and TiO_2-water nanofluids in the presence of a magnetic field. *Adv.Math.Phys.*,2014:1–9.

El-Zahar, E. R., Mahdy, A. E. N., Rashad, A. M., Saad, W., and Seddek, L. F. (2021). Unsteady mhd mixed convection flow of non-newtonian casson hybrid nanofluid in the stagnation zone of sphere spinning impulsively. *Fluids*, 6(6):197.

El-Zahar, E. R., Rashad, A. M., and Al-Juaydi, H. S. (2022). Studying massive suction impact on magneto-flow of a hybridized casson nanofluid on a porous continuous moving or fixed surface. *Symmetry*, 14(3):627.

El-Zahar, E. R., Rashad, A. M., Saad, W., and Seddek, L. F. (2020). Magneto-hybrid nanofluids flow via mixed convection past a radiative circular cylinder. *Sci. Rep.*, 10(1).

Hafeez, M., Hayat, T., Alsaedi, A., and Khan, M. I. (2021). Numerical simulation for electrical conducting rotating flow of Au (gold)-Zn (zinc)/EG (ethylene glycol) hybrid nanofluid. *Int. Commun. Heat Mass Transf.*, 124:105234.

Hayat, T., Muhammad, T., Shehzad, S., Chen, G., and Abbas, I. A. (2015). Interaction of magnetic field in flow of maxwell nanofluid with convective effect. *J. Magn. Magn. Mater.*, 389:48–55.

Hosseinzadeh, K., Afsharpanah, F., Zamani, S., Gholinia, M., and Ganji, D. (2018). A numerical investigation on ethylene glycol-titanium dioxide nanofluid convective flow over a stretching sheet in presence of heat generation/absorption. *Case Stud. Therm. Eng.*, 12:228–236.

Jaafar, A., Waini, I., Jamaludin, A., Nazar, R., and Pop, I. (2022). MHD flow and heat transfer of a hybrid nanofluid past a nonlinear surface stretching/shrinking with effects of thermal radiation and suction. *Chinese J. Phys.*, 79:13–27.

Jamaludin, A., Naganthran, K., Nazar, R., and Pop, I. (2020). MHD mixed convection stagnation-point flow of Cu-Al_2O_3/water hybrid nanofluid over a permeable stretching/shrinking surface with heat source/sink. *Eur. J. Mech. B Fluids.*, 84:71–80.

Jamaludin, A., Nazar, R., and Pop, I. (2018). Three-dimensional magnetohydrodynamic mixed convection flow of nanofluids over a nonlinearly permeable stretching/shrinking sheet with velocity and thermal slip. *Appl. Sci.*, 8(7):1128.

Jena, S., Mishra, S. R., and Pattnaik, P. K. (2020). Development in the heat transfer properties of nanofluid due to the interaction of inclined magnetic field and non-uniform heat source. *J. Nanofluids*, 9(3):143–151.

Jusoh, R., Nazar, R., and Pop, I. (2017). Flow and heat transfer of magnetohydrodynamic three-dimensional maxwell nanofluid over a permeable stretching/shrinking surface with convective boundary conditions. *Int. J. Mech. Sci.*, 124-125:166–173.

Jusoh, R., Nazar, R., and Pop, I. (2018). Three-dimensional flow of a nanofluid over a permeable stretching/shrinking surface with velocity slip: A revised model. *Phys. Fluids*, 30(3).

Khashi'ie, N. S., Arifin, N. M., Nazar, R., Hafidzuddin, E. H., Wahi, N., and Pop, I. (2020a). Magnetohydrodynamics (MHD) axisymmetric flow and heat transfer of a hybrid nanofluid past a radially permeable stretching/shrinking sheet with joule heating. *Chin. J. Phys.*, 64:251–263.

Khashi'ie, N. S., Arifin, N. M., Pop, I., Nazar, R., Hafidzuddin, E. H., and Wahi, N. (2020b). Three-dimensional hybrid nanofluid flow and heat transfer past a permeable stretching/shrinking sheet with velocity slip and convective condition. *Chin. J. Phys.*, 66:157–171.

Kumar, K., Ramesh, G., Gireesha, B., and Gorla, R. (2018). Characteristics of Joule heating and viscous dissipation on three-dimensional flow of Oldroyd B nanofluid with thermal radiation. *Alex. Eng. J.*, 57(3):2139–2149.

Kumbhakar, B. and Nandi, S. (2022). Unsteady mhd radiative-dissipative flow of Cu-Al_2O_3/H_2O hybrid nanofluid past a stretching sheet with slip and convective conditions: A regression analysis. *Math. Comput. Simul.*, 194:563–587.

Mahabaleshwar, U., Nagaraju, K., Sheremet, M., Baleanu, D., and Lorenzini, E. (2020). Mass transpiration on newtonian flow over a porous stretching/shrinking sheet with slip. *Chin. J. Phys.*, 63:130–137.

Mahdy, A., El-Zahar, E. R., Rashad, A. M., Saad, W., and Al-Juaydi, H. S. (2021). The magneto-natural convection flow of a micropolar hybrid nanofluid over a vertical plate saturated in a porous medium. *Fluids*, 6(6):202.

Mishra, S. R., Baag, S., Dash, G. C., and Acharya, M. R. (2019). Numerical approach to MHD flow of power-law fluid on a stretching sheet with non-uniform heat source. *Nonlinear Eng.*, 9(1):81–93.

Pattnaik, P., Mishra, S., Bég, O. A., Khan, U. F., and Umavathi, J. (2022). Axisymmetric radiative titanium dioxide magnetic nanofluid flow on a stretching cylinder with homogeneous/heterogeneous reactions in Darcy-Forchheimer porous media: Intelligent nanocoating simulation. *Mat. Sci. Eng. B*, 277:115589.

Pattnaik, P. K., Mishra, S. R., and Sharma, R. P. (2020). Numerical simulation for flow through conducting metal and metallic oxide nanofluids. *J. Nanofluids*, 9(4):354–361.

Pattnaik, P. K., Pattnaik, J. R., Mishra, S. R., and Nisar, K. S. (2021). Variation of the shape of Fe_3O_4-nanoparticles on the heat transfer phenomenon with the inclusion of thermal radiation. *J. Therm. Anal. Calorim.*, 147(3):2537–2548.

Rashad, A. M., Chamkha, A. J., Ismael, M. A., and Salah, T. (2018). Magnetohydrodynamics natural convection in a triangular cavity filled with a Cu-Al_2O_3/water hybrid nanofluid with localized heating from below and internal heat generation. *J. Heat Transf.*, 140(7).

Rashmi, M., Kola, R., Kumar, M., Pratyush, K., Dule, P., and Sivasankar, G. (2022). Investigation of heat transfer for silver oxide (Ag_2O) and iron oxide (Fe_3O_4) using nano fluid over a stretch sheet. *Mater. Today Proc.*, 69:1118–1125.

Rostami, M. N., Dinarvand, S., and Pop, I. (2018). Dual solutions for mixed convective stagnation-point flow of an aqueous silica–alumina hybrid nanofluid. *Chin. J. Phys.*, 56(5):2465–2478.

Sagheer, S., Farooq, U., and Hussain, M. (2023). Non-similar investigation of enhanced thermal efficiency of maxwell based hybrid nanofluid (MoS_2+ZnO) across a linearly stretched surface. *J. Magn. Magn. Mater.*, 565:170285.

Sakiadis, B. C. (1961). Boundary-layer behavior on continuous solid surfaces: I. boundary-layer equations for two-dimensional and axisymmetric flow. *AIChE J.*, 7(1):26–28.

Shampine, L. F., Gladwell, I., and Thompson, S. (2003). *Solving ODEs with MATLAB*. Cambridge University Press.

Sharma, R., Jha, A., Gaur, P., and Mishra, S. (2019). Nanofluid motion past a shrinking sheet in porous media under the impact of radiation and heat source/sink. *Int. J. Appl. Mech. Eng.*, 24(4):183–199.

Sheikholeslami, M. (2022a). Analyzing melting process of paraffin through the heat storage with honeycomb configuration utilizing nanoparticles. *J. Energy Storage*, 52:104954.

Sheikholeslami, M. (2022b). Numerical analysis of solar energy storage within a double pipe utilizing nanoparticles for expedition of melting. *Sol. Energy Mater. Sol. Cells*, 245:111856.

Sheikholeslami, M. (2022c). Numerical investigation of solar system equipped with innovative turbulator and hybrid nanofluid. *Sol. Energy Mater. Sol. Cells*, 243:111786.

Sheikholeslami, M. (2023). Efficacy of porous foam on discharging of phase change material with inclusion of hybrid nanomaterial. *J. Energy Storage*, 62:106925.

Sheikholeslami, M. and Al-Hussein, H. R. (2023). Analyzing efficiency of solar heat storage unit within a building including trombe wall equipped with phase change material in existence of fins. *J. Build. Eng.*, 71:106406.

Waqas, H., Farooq, U., Liu, D., Abid, M., Imran, M., and Muhammad, T. (2022). Heat transfer analysis of hybrid nanofluid flow with thermal radiation through a stretching sheet: A comparative study. *Int. Commun. Heat Mass Transf.*, 138:106303.